Energy and Information in Non-linear Systems

Aleš Gottvald (Editor)

Proceedings of
The 4th Japan-Central Europe Joint Workshop on Energy and Information in Non-linear Systems
November 10-12, 2000, Brno, Czech Republic

Organized in cooperation with:

Science and Technology Agency (Japan)
Japan International Science and Technology Exchange Center (Japan)
Japan Society of Applied Electromagnetics and Mechanics (Japan)
Czech Society of Applied Electromagnetics (CR)
Institute of Scientific Instruments, Academy of Sciences of the CR (CR)
Brno University of Technology (CR)

© Czech Society of Applied Electromagnetics, Brno (CR), 2001

Energy and Information in Non-Linear Systems (A. Gottvald, Ed.)
Proc. of the 4-th Japan-Central Europe Joint Workshop
© CSAEM, Brno (CR), 2001

FEM-BEM Coupling and Neural Network for Reconstruction of Crack Shape from Simulated Pulse Eddy Current Signals

Gabriel Preda, Ovidiu Mihalache, Bogdan Cranganu-Cretu*, Zhenmao Chen* and Kenzo Miya
Nuclear Engineering Research Laboratory, Graduate School of Engineering,
The University of Tokyo, Tokai-mura, Naka-gun, Ibaraki 319-1106, Japan
* JSAEM, SB Bldg. 801, 1-4-6 Nezu, Bunkyo-ku, Tokyo 113-0031, Japan
E-mail:preda@tokai.t.u-tokyo.ac.jp

Abstract- Pulse eddy-currents is proposed as a NDT technique to detect flaws in conductive structures with large thickness. The harmonic component of pulse is rich, thus the pick-up signal contains the amount of information equivalent to a multi-frequency analysis. Due to the short time length of the pulse, the amplitude of the pick-up signal can be increased through increasing excitation. Both direct simulation of pulse eddy-currents phenomena using an A-φ FEM-BEM code and Neural Networks-based inversion techniques are performed. Numerical results for the inversion of signals due to outer defects are shown.

1. INTRODUCTION

Eddy current testing (ECT) using sinusoidal mode has been extensively used for detection of flaws in metallic structures such as SG tubing in PWR power plants. Despite its advantages as high speed and reliability to in-service inspection, this method is limited by skin effect only to thin, non-magnetic structural components. A possible alternative is the use of pulse eddy-currents. This option provides a multifold advantage: the rich harmonic component of a pulse accounts for a multi-frequency analysis, the lower harmonics penetrating deeper in the structure, while the short duration of a signal allows an increase in the power for the same cumulated heat and consequently thermal exposure of the coil-specimen system [1-2]. The present study enhances the possibility of crack shape reconstruction using simulated pulse eddy-current signals. The inverse procedure uses Neural Networks [4] and additional regularization methods as shifting aperture [5] and Principal Component Analysis (PCA).

2. NUMERICAL FORMULATION FOR FORWARD PROBLEM SIMULATION

A FEM-BEM coupling, based on A-φ formulation for transient eddy-currents was developed. The rationale for this formulation, previously used for AC analysis, is extensively developed in [3]. From Maxwell equations in the limits of quasistatic field and using the Coulomb gauge ∇·A=0, the governing equations are obtained:

$$-\frac{1}{\mu_0}\Delta\mathbf{A}-\sigma\left(\frac{\partial\mathbf{A}}{\partial t}+\nabla\frac{\partial\phi}{\partial t}\right)=0 \quad in\,\Omega_c, \tag{1}$$

$$\nabla\cdot\sigma\left(\frac{\partial\mathbf{A}}{\partial t}+\nabla\frac{\partial\phi}{\partial t}\right)=0 \quad in\,\Omega_c, \tag{2}$$

$$-\frac{1}{\mu_0}\Delta\mathbf{A}=\mathbf{J}_0 \quad in\,\Omega_0, \tag{3}$$

where $\Omega = \Omega_c \cup \Omega_0$ is an unbounded domain, Ω_c is the conductive domain and Ω_0 is the air. The sources of magnetic field are the impressed current sources $\mathbf{J}_0$ in the air. On the interface between FEM-domain (conductive) and BEM-domain (air) the tangential component of **H** is continuous:

$$\left.\frac{1}{\mu_0}\frac{\partial\mathbf{A}}{\partial\mathbf{n}}\right|_{FEM}=\left.\frac{1}{\mu_0}\frac{\partial\mathbf{A}}{\partial\mathbf{n}}\right|_{BEM} \tag{4}$$

Using Galerkin approach, equations (1-3) are discretized by projecting each term of the equations on the shape functions and integrating over the entire problem domain Ω. The equation system obtained after FEM-BEM coupling using interface condition (4) is:

$$[K_{tot}]\{\mathbf{A}\}+[Q]\begin{Bmatrix}\partial A/\partial t\\ \partial\phi/\partial t\end{Bmatrix}=[D][G]^{-1}\{F_0\}, \quad (5)$$

where K_{tot} and Q are banded, partially full matrices and D is the distribution matrix used in the BEM method. A Crank-Nicholson integration scheme with constant time step and $\theta = 1/2$ is used and a linear system is solved every time step.

3. SIMULATION SET-UP AND SENSITIVITY ANALYSIS

Based on the approach described above, a code was implemented and used to investigate the application of pulse eddy-currents to detection of flaws in thick conductive structures. The simulation set-up is described in Fig. 1. A pancake coil is used to energize the specimen and a Hall sensor for pick-up the z-component of magnetic flux density under the axis of coil. The system pancake probe-Hall sensor shows less sensitivity to frequency variation than the classic auto-induction pancake used in AC detection [2]. In the case of AC, the pancake probe is optimized for a certain frequency. In the case of pulse eddy-current excitation, due to the rich harmonic component of the signal, such a frequency-optimization technique is hampered. The simulations were performed for a 50 mm × 50 mm square, 10 mm thick non-ferromagnetic plate, with conductivity $\sigma = 10^6$ S/m, using a single pulse with duration less than 0.1 ms (80 μs, time t=10...90 μs), with rise time 10 μs (rise and fall exponentially), recurrence frequency 100 Hz and amplitude I_{max} = 2500 AT (100 A/mm^2). The pancake coil have the dimensions: external radius R_{max}= 6 mm, internal radius R_{min} = 1 mm and height Z = 5 mm. The coil lift-off is 1 mm, the pick-up sensor lift-off is 0.5 mm. In this simulation, time step is 1 μs; 110 steps were simulated. Scan velocity admitted is 0.1m/s with a scan pitch of 1 mm.

Figure 2 shows the pick-up signal due to eddy-currents, i.e. the B_z component of magnetic flux density on the scan point. Difference signals are shown in Fig. 3. Due to phase shifting, the maximum amplitude of difference signal is reached at different times for different crack depths [2]. We noticed that the maximum value of the difference signal due to 80% OD crack was reached at t=32 μs, at 45 μs for 60% OD cracks and at 50 μs for 40% OD crack. Consequently, the sample time should be chosen in order to emphasize signals from larger cracks but keeping still detectable smaller crack, in this case the sample time will be at t = 40 μs. In Fig. 4 is shown the B-scan on line y=[-6:6] mm, x=0, z= 0.5 mm over the plate. In Fig. 5,a is plot the difference signal for 10 mm long, 0.2 mm width, OD cracks with depth ranged from 40% to 80% and in Fig. 5,b for a 0.2mm width, 60% OD crack, with lengths ranged from 2 to 10 mm.

4. INVERSION OF SIGNALS FOR RECONSTRUCTION OF CRACK SHAPE

The inverse method aims to discover the signal-to-shape relationship from a set of non-uniformly distributed examples. In addition to a statistical analysis and transformation of input data, by Principal Component Analysis (PCA), and NN with incremental learning, a special data fragmentation-data fusion technique is used. The procedure was extensively presented elsewhere [5]. The network contains a single hidden layer, and additional direct connections between inputs and outputs. The training starts with only one hidden node, and for each training epoch a new node is created, the new input-hidden connections receive random weights and the rest of the weights are solved by a least-square minimization using singular value decomposition. The training algorithm of the employed NN implies least-squares solutions of an over-determined equation system at each iteration (training epoch):

$$\left[\mathbf{A} \quad f_1(\mathbf{A}\cdot\mathbf{W}_{ih})\right]\cdot\begin{bmatrix}\mathbf{W}_{io}\\ \mathbf{W}_{ho}\end{bmatrix}=f_2^{-1}(\mathbf{B}) \quad (6)$$

where **A**, **B** represent the input, and output training sets, respectively, f_1 and f_2, the nonlinear activation functions for the hidden and output nodes, $\mathbf{W}_{ih}$ is a randomly generated, fixed coefficient matrix, and $\mathbf{W}_{io}$, $\mathbf{W}_{ho}$ are the matrices containing the unknowns of the problem, *i.e.*, the input-output and the hidden-output interconnection weights, respectively.

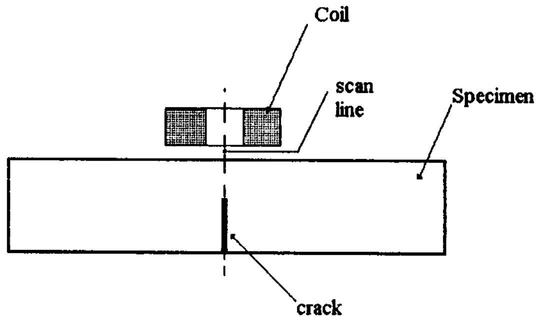

Fig. 1 Simulation set-up

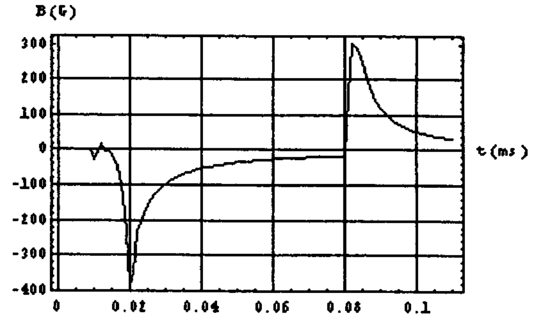

Fig. 2 Time variation B_z component of the pick-up signal due to reaction eddy-current, in the case of plate without crack. Measurement point centered over the crack

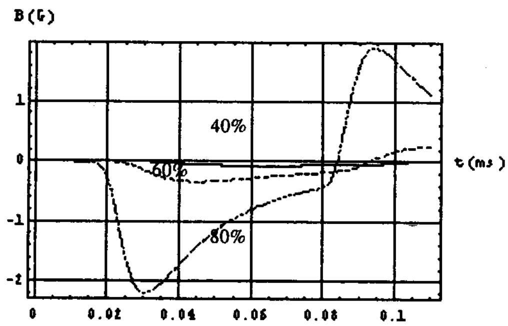

Fig. 3 Difference signal for a crack 10mm length, 0.2 mm width, 40%, 60%, 80 % depth.

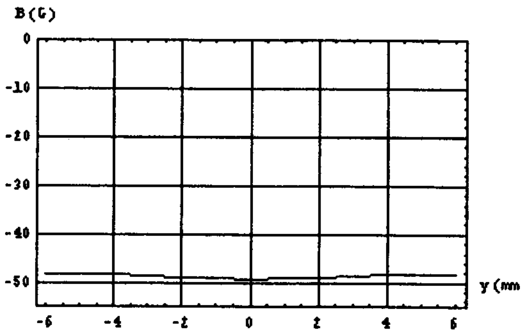

Fig. 4 Signal for B-scan on line [-6:6] mm, x=0, z= 0.5 mm over the plate; no-crack case; value of signal at sample moment t = 40 µs.

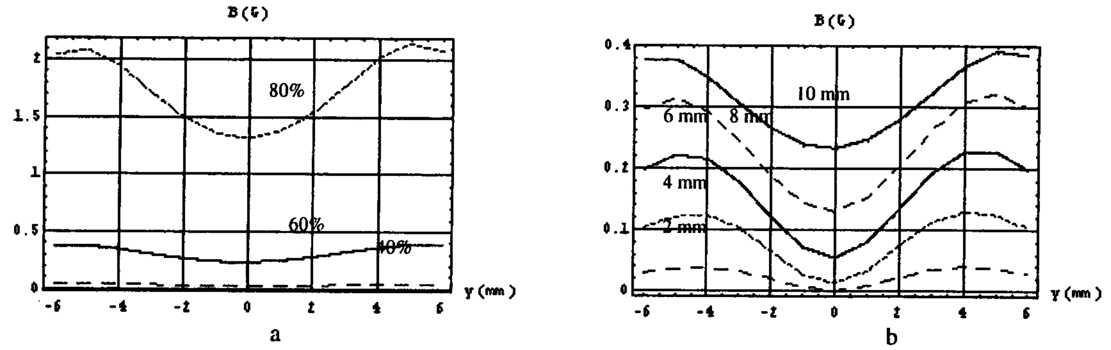

Fig. 5 a) Difference signal for 10mm length, 0.2 mm width OD crack 40%, 60% and 80% depth.
b) Difference signal for 60% depth, 0.2 mm width, with length ranged from 2 to 10 mm.

The crack was parameterized at a cell level. To each element in the analyzed region is associated one value, 1 for non-vanished conductivity, 0 for vanishing conductivity. The cells values in the analyzed region represent the outputs of the network and the signal values in the scanning points the inputs. The I-O pairs of the initial database are partitioned into training, validation and verification sets. The validation set is used only to control the training optimality, by monitoring the currently achieved estimation error. The shifting aperture technique roles are to reduce the ill-posedness of the map, to minimize the dimension of the mapping problem and to multiply the number of available cases [5]. 250 longitudinal scans were simulated along the same number of OD cracks in a plate specimen as described in section 3. Each complete scan consisted of 13 sensor readings along a probing line parallel to the crack mouth, with 1mm pitch. Apertures of 5 elements with 6 scan points were taken. In this way were formed a total of 2000 such input-output vector pairs. From this maximal database, validation and verification sub-sets were extracted and used only in the testing phase. 1760 I-O pairs were used for training, 160 for validation and 80 for verification (test) set. The variation of the average deviations for validation set, of learning error and of the quality parameter with training epochs is shown in Fig. 6. The training was stopped after about 550 epochs, the minimal validation error being obtained for epoch 236. The mapping was obtained by training with unjittered signals. In Fig. 7, four reconstruction examples, are presented in gray-level images. For each estimation the correct image is given besides. Each image represents a 12mm long profile, which is obtained by a weighted superposition of 8 successive windows, each cell value being obtained by superposition of 1 to 5 cell values with different weights.

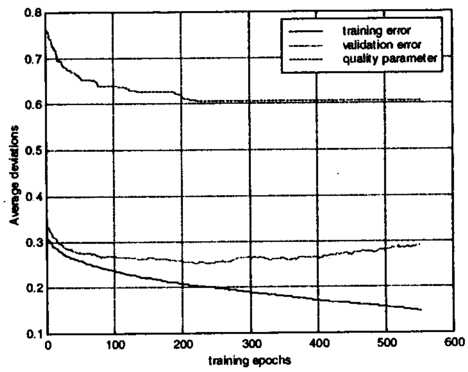

Fig. 6 Average deviations vs. training epoch

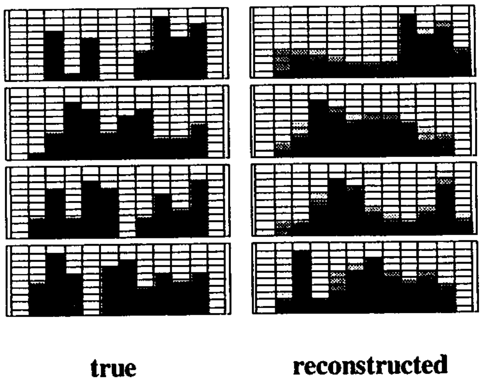

Fig. 7 Reconstruction from noise-free data

5. CONCLUSIONS

The above experiments showed that the method proposed give good results for detection of crack in thick conductive structures. The optimum sample time depends, due to phase shifting, on the depth of the crack. An inverse procedure, based on Neural Networks and various regularization method is used for reconstructing the shape of the crack from sampled signals during B-scan with a pancake coil for excitation and Hall-sensor pick-up system. The promising results encourage us to tackle the more difficult problems of pulse eddy-currents in interaction with ferromagnetic structures.

REFERENCES

[1] M. Gibbs and J. Campbell, Pulsed Eddy Current Inspection of Cracks under Installed Fasteners, *Material Evaluation*, Vol. 46, January 1991, pp. 51-59.

[2] C.V. Dodd, W.E. Deeds and L.D. Chitwood, Eddy Current Inspection of Ferromagnetic Materials Using Pulsed Magnetic Saturation, *Material Evaluation*, Vol. 46, November1988, pp. 1592-1597.

[3] Z. Chen and K. Miya, ECT Inversion Using a Knowledge-Based Forward Solver, *J. Nondestr. Eval.*, Vol. 17, No. 3, 1998, pp. 167-175.

[4] C.L.P.Chen, A Rapid Supervised Learning Neural Network for Function Interpolation and Approximation, *IEEE Trans Neural Networks*, Vol. 7, 1996, pp.1220-1230.

[5] R.C.Popa and K.Miya, Approximate inverse mapping in ECT, based on aperture shifting and neural network regression, *J. Nondestr. Eval.*, Vol. 17., No. 4, 1998, pp. 209-221.